Structural basis for recruitment of mitochondrial fission complexes by Fis1

Yan Zhang and David C. Chan*

Division of Biology, California Institute of Technology, 1200 East California Boulevard, MC 114-96, Pasadena, CA 91125

Edited by Giuseppe Attardi, California Institute of Technology, Pasadena, CA, and approved September 28, 2007 (received for review July 9, 2007)

Mitochondrial fission controls mitochondrial shape and physiology, including mitochondrial remodeling in apoptosis. During assembly of the yeast mitochondrial fission complex, the outer membrane protein Fis1 recruits the dynamin-related GTPase Dnm1 to mitochondria. Fis1 contains a tetratricopeptide repeat (TPR) domain and interacts with Dnm1 via the molecular adaptors Mdv1 and Caf4. By using crystallographic analysis of adaptor-Fis1 complexes, we show that these adaptors use two helices to bind to both the concave and convex surfaces of the Fis1 TPR domain. Fis1 therefore contains two interaction interfaces, a binding mode that, to our knowledge, has not been observed previously for TPR domains. Genetic and biochemical studies indicate that both binding interfaces are important for binding of Mdv1 and Caf4 to Fis1 and for mitochondrial fission activity *in vivo*. Our results reveal how Fis1 recruits the mitochondrial fission complex and will facilitate efforts to manipulate mitochondrial fission.

apoptosis | mitochondrial division | mitochondrial dynamics | tetratricopeptide repeat

Mitochondrial dynamics has emerged as an important process controlling mitochondrial shape, size, distribution, and physiology (1, 2). Mitochondrial fission, balanced by the opposing process of fusion, controls the morphology of mitochondria. Increased fission leads to mitochondrial fragmentation, whereas reduced mitochondrial fission causes elongation and increased connectivity of mitochondria.

Recent results indicate that mitochondrial fission has important physiological functions. In humans, loss of mitochondrial fission results in neonatal lethality with microcephaly, developmental delay, and metabolic aberrations (3). Defects in mitochondrial fission also disrupt mitochondrial distribution in neurons and result in defective synaptic transmission (4). Moreover, mitochondrial fission regulates apoptosis in yeast (5), worms (6), flies (7, 8), and mammals (9). In the early stages of apoptosis, recruitment of fission complexes to mitochondria is increased. The increase in fission leads to mitochondrial fragmentation, which appears to be important for execution of death programs (10). Therefore, a structural and mechanistic understanding of mitochondrial fission may facilitate efforts to regulate apoptosis.

The molecular basis for recruitment of the mitochondrial fission machinery is best understood in budding yeast (2). Mitochondrial fission complexes assemble on the mitochondrial outer membrane protein Fis1 (11–13). Fis1 mediates the assembly of fission complexes consisting of adaptors (Mdv1 or Caf4) and the Dnm1 GTPase, a dynamin-related protein (14–17). Dnm1 is predominantly found in puncta on the mitochondrial surface, and these puncta mark potential sites of future fission. Mdv1p and Caf4p are soluble proteins containing an N-terminal extension, a coiled-coil region, and a COOH-terminal seven-WD40 repeat domain. Acting as molecular adaptors, these proteins bind to Fis1p through the N-terminal extension region and to Dnm1p through the WD40 region (14, 15, 17). Mdv1 and Caf4 are redundant in their ability to work with Fis1 to recruit Dnm1 to mitochondria. *mdv1*Δ and *caf4*Δ mutants show largely normal Dnm1 localization, but *mdv1*Δ *caf4*Δ mutants, like *fis1*Δ mutants, show cytosolic localization of Dnm1 (15). Mdv1 is more active than Caf4 in promoting fission.

Because Fis1 initiates assembly of the mitochondrial fission complex, an important mechanistic issue is how Fis1 binds its ligands, Mdv1 and Caf4. The cytosolic domain of Fis1 forms a six-helix bundle, in which the central four helices consist of two tandem tetratricopeptide repeat (TPR)-like motifs. The TPR is a helix-turn-helix motif that is typically organized into a tandem array (18). Such tandem TPR motifs make a right-handed superhelical structure with a concave surface. In all of the solved TPR domains bound to ligand, the ligands are bound in a hydrophobic groove on the concave surface (18–21). The ligands are either helical or in an extended conformation with their axes parallel to the hydrophobic groove.

Given this strong precedent, it has been widely assumed that Fis1 would also bind its ligands through the hydrophobic groove identified on the concave surface of the TPR fold (22–24). In yeast Fis1, surprisingly, the extreme N-terminal residues (termed the N-terminal arm) form a short helix that lies in this predicted ligand-binding site. Therefore, it has been proposed that the N-terminal arm of yeast Fis1 might regulate the binding of Mdv1 and Caf4 to the concave surface (24). Indeed, the N-terminal arm of yeast Fis1 is important for Fis1 function (16, 24). We determined the atomic structure of a Fis1/Mdv1 and a Fis1/Caf4 complex. These structures reveal, in contrast to the previous models, that the TPR domain of Fis1 is used in a unique way to recruit Mdv1 and Caf4. These ligands use a helix–loop–helix motif to pack against both the concave and convex surfaces of the Fis1 TPR domain. Cellular analyses support the physiological significance of these dual molecular interactions. Sequence analysis indicates that mammalian Fis1 probably uses a similar strategy to bind ligands during apoptosis.

Results

Fis1 Binds Ligands in a Manner Distinct from Other TPR Domain Proteins. To understand how Fis1 interacts with the two adaptor proteins, we crystallized complexes of Fis1 (the cytosolic domain, residues 1–129) bound to an N-terminal fragment of Mdv1 (residues 122–171; 2.15 Å) or Caf4 (residues 81–140; 1.9 Å) (Table 1). The binding of Fis1 to adaptors contained several unanticipated features. The Fis1 structures in the two complexes are almost identical to unliganded Fis1 (24). In all cases, helices α1–α6 formed the core six-helix bundle, with α2/α3 and α4/α5 forming tandem TPR-like motifs that lined a hydrophobic,

Author contributions: Y.Z. and D.C.C. designed research; Y.Z. performed research; Y.Z. and D.C.C. analyzed data; and Y.Z. and D.C.C. wrote the paper.

The authors declare no conflict of interest.

This article is a PNAS Direct Submission.

Abbreviation: TPR, tetratricopeptide repeat.

Data deposition: The atomic coordinates and structure factors have been deposited in the Protein Data Bank, www.pdb.org (PDB ID codes 2PQN and 2PQR).

*To whom correspondence should be addressed. E-mail: dchan@caltech.edu.

This article contains supporting information online at www.pnas.org/cgi/content/full/0706441104/DC1.

Table 1. Crystallographic data and refinement statistics

	Fis1/Mdv1	Fis1/Caf4
Data collection		
Space group	*P*2(1)2(1)2	*P*2(1)
Cell dimensions		
a/*b*/*c*, Å	43.17/57.39/69.80	60.41/46.95/64.47
$\alpha/\beta/\gamma$, °	90/90/90	90/99.21/90
Redundancy	5.7 (4.3)	3.7(3.4)
Completeness, %	98.6 (89.5)	99.3 (98.3)
R_{sym},* %	6.3 (35.9)	7.3 (42.4)
I/σ	23.2 (3.3)	17.7 (2.5)
Refinement statistics		
Resolution, Å	29.81–2.15	50–1.90
R_{work}/R_{free},†‡ %	19.8/23.3	20.8/24.1
Number of atoms		
Protein	1189	2523
Ligand/ion	0	3
Water	41	141
B factors		
Protein	43.3	34.8
Ligand/ion	NA	45.7
Water	44.3	39.7
rmsds		
Bonds lengths, Å	0.016	0.016
Bond angels, °	1.5	1.5

NA, not available. Values for the outer resolution shell are given in parentheses.

*$R_{sym} = \Sigma\Sigma_i|I_i - \langle I\rangle|/\Sigma\langle I\rangle$, where $\langle I\rangle$ is the mean intensity of N reflections with intensities I_i and common indices *h*, *k*, and *l*.

†*R* factor $= \Sigma_{hkl}||F_{obs}| - |F_{cal}||/\Sigma_{hkl}|F_{obs}|$, where F_{obs} and F_{cal} are the observed and calculated structure factors, respectively.

‡For R_{free}, the sum is extended over a subset of reflections (5%) excluded from all stages of refinement.

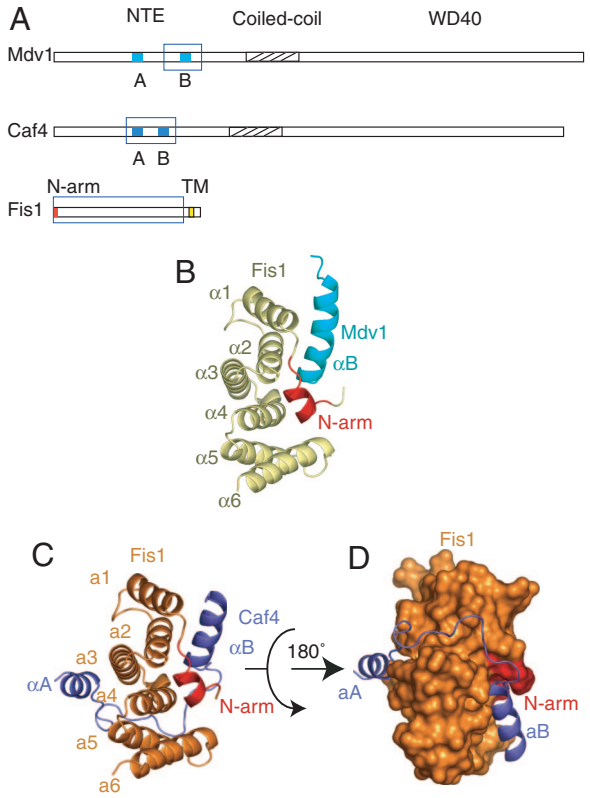

Fig. 1. Structures of Fis1/Mdv1 and Fis1/Caf4 complexes. (*A*) Domain arrangement of Mdv1, Caf4, and Fis1. Regions A and B in Caf4, located in the N-terminal extension, directly bind Fis1, as shown in the crystal structure (*C*). The corresponding region B and the predicted region A in Mdv1 are also labeled. For each protein, the region within the blue frame is present in the crystallization studies. (*B*) Crystal structure of the Fis1/Mdv1 complex depicted in a ribbon representation. The Fis1 N-terminal arm (red) remains packed against the original hydrophobic groove and stabilizes the αB helix of Mdv1 (cyan), which packs against a second hydrophobic groove on the concave surface of Fis1. (*C*) Crystal structure of the Fis1/Caf4 complex. In addition to the αB helix packed against the concave Fis1 surface, Caf4 (purple) uses the αA helix and the intervening loop to bind the convex Fis1 surface. (*D*) The Fis1/Caf4 structure with Fis1 shown in a surface representation. The long loop allows Caf4 to straddle both sides of the Fis1 TPR domain.

concave surface (Fig. 1 *B* and *C*). Previous models have proposed that ligand binding would require relocation of the Fis1 N-terminal arm to provide access to the binding pocket (16, 24). However, the crystal structures revealed that the Fis1 N-terminal arm remained packed against the hydrophobic groove (Fig. 1 *B–D*). This was possible because, surprisingly, Mdv1 and Caf4 did not contact the predicted binding pocket but instead bound to a different region of the concave surface. Residues 147–163 of Mdv1 formed an α-helix (helix αB) that packed into a second hydrophobic groove oriented approximately orthogonal to the original hydrophobic groove occupied by the Fis1 N-terminal arm (Fig. 1 *A* and *B*). The Fis1 N-terminal arm stabilized the binding of helix αB by packing against the N terminus of the helix. The total surface area buried at the Fis1/αB interface was 1,420 Å^2.

Remarkably, the Fis1/Caf4 structure revealed an additional major protein–protein interface. Helix αB of Caf4 bound to Fis1 in the same manner as Mdv1 (Fig. 1 *A*, *C*, and *D*), but an additional helix (helix αA) further N-terminal packed into the convex side of the Fis1 helical bundle. Caf4 helix αA lay in a shallow groove lined by helices α3 and α5 of Fis1. Helices αA and αB were connected by an extended loop that enabled these helices to crossover and bind to opposite surfaces of Fis1 (Fig. 1 *C* and *D*). Therefore, the U-shaped αA–loop–αB region of Caf4 simultaneously bound both surfaces of Fis1, increasing the buried surface area to 3,111 Å^2.

The TPR domain is a widely used protein interaction domain that is found in >800 proteins (18). To date, available structures of TPR-containing proteins complexed with ligands show protein–protein interactions occurring only at the concave surface (19–21). Therefore, our Fis1/Caf4 structure revealed the flexibility of the TPR domain in mediating protein–protein interactions and may represent a distinct structural class of TPR-containing proteins.

Helices αA and αB of Mdv1 and Caf4 Are Necessary and Sufficient for Their Interaction with Fis1. Given our ability to produce Fis1/Mdv1 crystals from an Mdv1 fragment lacking helix αA, it was imperative to determine the role of helix αA in normal Mdv1 and Caf4 function. The key residues involved in the binding of Caf4 αA and αB to Fis1 were all conserved in Mdv1 (Fig. 2*A*). To experimentally test the contribution of helices αA and αB to the binding of Mdv1 and Caf4 to Fis1, we used the yeast two-hybrid assay, which has been shown previously to recapitulate Fis1 protein–protein interactions (15). Although the N-terminal half of Caf4 interacted with Fis1, this interaction could not be reconstituted with Caf4 αA or αB alone (Fig. 2*B*). In contrast, a fragment containing Caf4 αA and αB interacted as efficiently as the entire N-terminal half. Similar interaction patterns were observed between Mdv1 and Fis1. These results indicate that for both Mdv1 and Caf4, the U-shaped αA–loop–αB region constitutes the minimal Fis1-binding domain. Moreover, the results suggest that the Mdv1 fragment (residues 122–171) used for crystallization does not contain the full, high-affinity Fis1-

CELL BIOLOGY

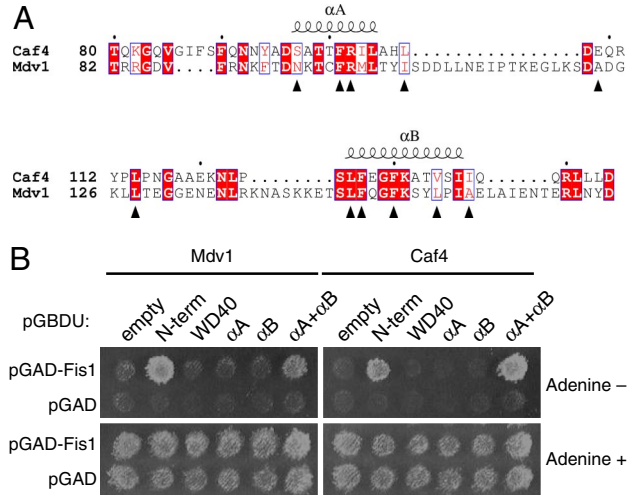

Fig. 2. The two binding sites on Mdv1 and Caf4 are necessary and sufficient for binding to Fis1. (*A*) Sequence alignment of a portion of the N-terminal extension region (N-term) of Mdv1 and Caf4. Sequences constituting binding sites αA and αB are indicated, and residues contacting Fis1 are highlighted by black triangles. Identical residues are white with a red background, and similar residues are red with a blue frame. (*B*) Yeast two-hybrid assay. Fis1 expressed from the pGAD vector was tested against Mdv1 or Caf4 constructs containing the N-terminal region, the C-terminal region (WD40), αA alone, αB alone, or αA and αB. Growth on adenine-deficient plates indicates an interaction.

binding region. However, the fragment bound under the high concentrations used in crystallography.

Mutations in Helices αA or αB of Mdv1 and Caf4 Disrupt Their Interaction with Fis1, Leading to Loss of Mitochondrial Fission Activity. To establish the biological significance of these protein interfaces, we mutated key residues in the binding sites of Mdv1 and Caf4. Mdv1 helix αB made hydrophobic contacts with Fis1, with the most prominent interactions mediated by residues L148, F149, and F152 (Fig. 3*A*). Mdv1 L148 contacted the aromatic ring of Fis1 F43. Mdv1 F149 stacked against Fis1 P8 and the indole ring of W47. Finally, Mdv1 F152 contacted Fis1 W47, L17, and L25. In Caf4, analogous αB residues (L126, F127, and F130) made similar contacts. In immunoprecipitation experiments, alanine mutations at each of these positions abolished binding of Mdv1 and Caf4 to Fis1 (Fig. 3 *C* and *D*).

Mutational analysis further demonstrated the importance of helix αA in not only Caf4 but also Mdv1. Several Caf4 helix αA–loop residues, including F101, R102, and L107, made extensive contacts against Fis1 (Fig. 3*B*). Caf4 F101 had hydrophobic contacts with Fis1 V62 and L90, and R102 formed hydrogen bonds with Fis1 E92. Caf4 L107 was in the loop region and lay in a hydrophobic pocket lined by Fis1 Y69, L80, and Y99. We mutated these Caf4 residues (F101A/R102A, L107A) and the corresponding Mdv1 residues (F99A/R100A, I105A) to alanine. In each case, the mutants failed to coimmunoprecipitate with Fis1 (Fig. 3 *C* and *D*). Taken together, these binding results indicate that both helices αA and αB are essential for the binding of Mdv1 and Caf4 to Fis1 under physiological expression levels.

We further analyzed the Mdv1 mutants for localization to mitochondria and mitochondrial fission activity. Whereas the majority (80%) of cells expressing a wild-type GFP–Mdv1 fusion protein showed punctate fluorescence on mitochondria, all of the mutant GFP–Mdv1 constructs yielded uniform cytosolic fluorescence in all cells, with no obvious concentration on mitochondria (Fig. 3*E*). Consistent with this mislocalization, all of the Mdv1 mutants were deficient in promoting mitochondrial fission (Fig. 3*F*). In the mitochondrial fission assay, the Mdv1 αB

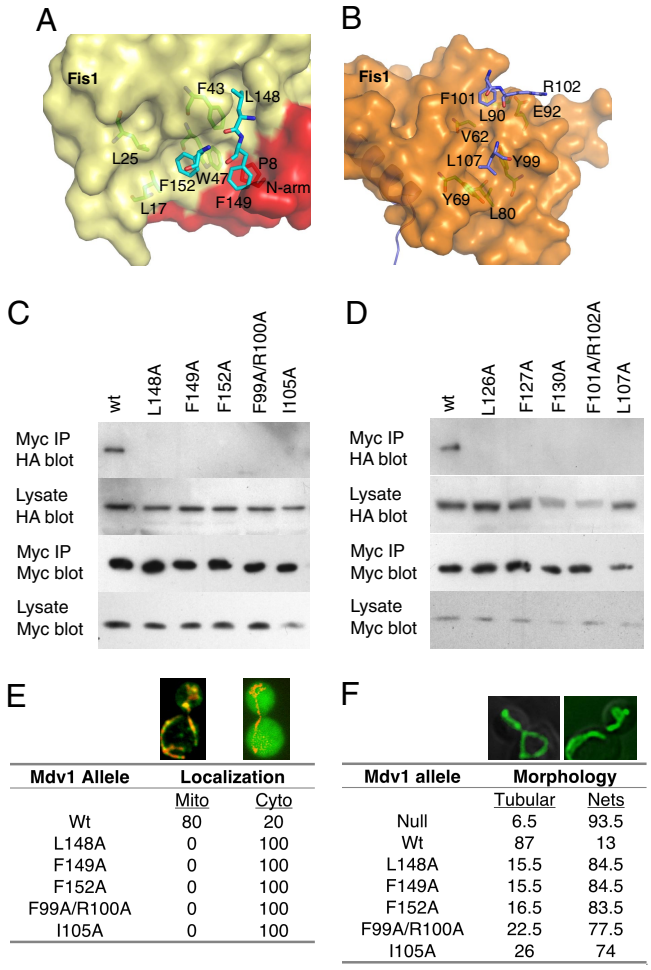

Mdv1 Allele	Localization	
	Mito	Cyto
Wt	80	20
L148A	0	100
F149A	0	100
F152A	0	100
F99A/R100A	0	100
I105A	0	100

Mdv1 allele	Morphology	
	Tubular	Nets
Null	6.5	93.5
Wt	87	13
L148A	15.5	84.5
F149A	15.5	84.5
F152A	16.5	83.5
F99A/R100A	22.5	77.5
I105A	26	74

Fig. 3. The αA and αB helices are essential for adaptor function. (*A*) Interactions of Mdv1 αB residues with Fis1. Fis1 is shown in a surface representation with key residues highlighted. Mdv1 αB residues (cyan) are shown in a stick representation. (*B*) Interactions of Caf4 αA residues with Fis1. (*C*) Immunoprecipitation of HA-tagged Mdv1 mutants with Myc-tagged Fis1. (*D*) Immunoprecipitation of HA-tagged Caf4 mutants with Myc-tagged Fis1. (*E*) Subcellular localization of Mdv1 mutants. The localization of GFP–Mdv1 was scored by comparing to mito-DsRed in yeast carrying the indicated Mdv1 mutation. Representative examples of mitochondrial and cytoplasmic localization are shown. (*F*) Rescue of *mdv1*Δ yeast with Mdv1 mutants. Mitochondria in cells expressing the indicated Mdv1 constructs were scored with mitochondrially targeted GFP. In all phenotypic characterizations, 200 cells were scored, and percentages are shown. Representative examples of yeast with tubular and net-like mitochondria are shown.

helix mutants were more strongly affected than the αA helix mutants. Our results indicate that helices αA and αB are both important for the mitochondrial localization and fission activity of Mdv1.

Because deletion of Caf4 has no obvious effect on mitochondrial morphology (15), we were unable to assay the effect of the Caf4 mutations on Caf4 activity. However, by analyzing a GFP–Caf4 fusion protein, we could examine their effects on Caf4 localization. We found that the Caf4 αB helix mutants L126A and F130A were strongly deficient in mitochondrial localization but that the αA helix mutants F101/R102A and L107A were not significantly affected (data not shown). Taken together with the Mdv1 data, these results suggest that helix αB may contribute somewhat more to the binding interface with Fis1 than helix αA.

A

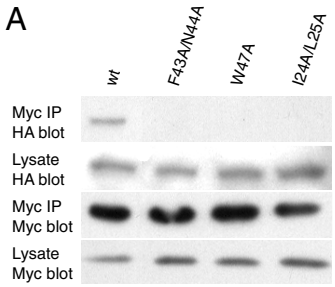

B

Fis1 allele	Morphology		Dnm1 localization	
	Tubular	Nets	Mito	Cyto
fis1Δ	0	100	0	100
Wt	79	27	78	22
F43A/N44A	7.5	92.5	11	89
W47A	7.5	92.5	11	89
I24A/L25A	29	71	21	79

C

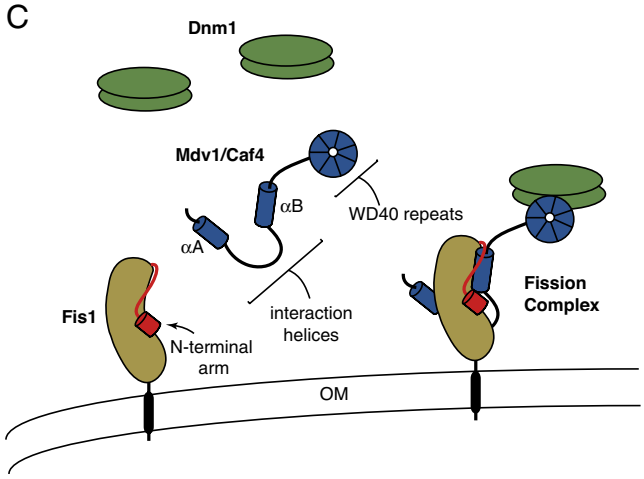

Fig. 4. Surface residues essential for Fis1 function. (*A*) Immunoprecipitation of HA-tagged Mdv1 by Myc-tagged Fis1 containing mutations in surface residues contacting the αB helix of adaptors. wt, wild type. (*B*) Ability of Fis1 mutants to rescue mitochondrial morphology and Dnm1 recruitment in *fis1Δ* yeast. Mitochondrial morphology was scored by using mito-DsRed. Subcellular localization of GFP–Dnm1 puncta was scored by comparison with mito-DsRed. (*C*) Schematic of fission complex recruitment by Fis1. In the unliganded state (shown at left), Fis1 resides in the mitochondrial outer membrane (OM) with its N-terminal arm (red region) packed against the concave surface of the TPR domain. The adaptors Mdv1 and Caf4 use two N-terminal helices to bind Fis1. The Fis1 N-terminal arm stabilizes adaptor binding by interacting with the αB helix (complex shown at right). The WD40 region of the adaptors then recruits Dnm1 to the mitochondria. Dnm1 exists as dimers and is activated by assembly into higher-order oligomers (not shown).

Fis1 Residues Lining the αB-Binding Groove Are Essential for Mitochondrial Fission and Recruitment of Mdv1 and Dnm1. Our structural studies indicated that helix αB in Mdv1 and Caf4 bound to the concave face of Fis1 but to a different hydrophobic groove than previously predicted. To experimentally evaluate the functional significance of this Fis1 groove, we mutated key Fis1 residues lining this groove to alanine (I24A/L25A, F43A/N44A, and W47A). In contrast to wild-type Fis1, none of the Fis1 mutants was able to coimmunoprecipitate Mdv1 (Fig. 4*A*). Moreover, each of the Fis1 mutants showed greatly reduced ability to support mitochondrial fission when expressed in *fis1Δ* cells (Fig. 4*B*). Consistent with this loss of mitochondrial fission activity, the Fis1 mutants were unable to recruit Dnm1 puncta to mitochondria (Fig. 4*B*). Because Mdv1 and Caf4 play redundant roles in Dnm1 recruitment to mitochondria (15), these results indicate that Fis1 with mutations at the αB-binding site are deficient for binding both Mdv1 and Caf4, as predicted by our crystal structures.

Discussion

Mitochondrial fission is a conserved, fundamental cellular process that regulates mitochondrial shape and function. Fis1 anchors fission complexes onto the mitochondrial outer membrane. In yeast, Mdv1 and Caf4 bridge the interaction between Fis1 and Dnm1, a mechanochemical enzyme thought to constrict mitochondrial tubules during fission. Our current results reveal the structural basis of recruitment of these adaptor molecules by Fis1. Caf4, and by inference Mdv1, uses a helix–loop–helix motif to clasp both the concave and convex surfaces of Fis1 (Fig. 4*C*). Biochemical and cytological studies demonstrate that key interactions revealed in the structures are critical for maintaining assembly of mitochondrial fission complexes and normal mitochondrial morphology *in vivo*. Our conclusions are supported by previous work showing that Mdv1L148P, analogous to our αB helix mutant L148A (Fig. 3), is defective for Fis1 binding, mitochondrial localization, and fission activity (25).

These structural insights clarify previous findings. In the unliganded structure of yeast Fis1, it has been perplexing that the N-terminal arm lies in the presumed ligand-binding site (24). This observation has led to suggestions that the N-terminal arm likely relocates to allow ligand binding (16, 24). In contrast, our structures indicate that the presence of the N-terminal arm is fully compatible with Mdv1 or Caf4 binding, because these ligands bind unexpectedly to an adjacent site. Deletion of the N-terminal arm of Fis1 greatly reduces mitochondrial fission (16, 24), but this defect can be complemented by overexpression of Mdv1 (16). Based on the structural data here, helix αB of Mdv1 binds to a different hydrophobic groove than anticipated, and this interaction is facilitated by packing interactions against the N-terminal arm of Fis1 (Fig. 4*C*). Therefore, deletion of the N-terminal arm would weaken Mdv1 binding, a defect that can be overcome by increasing the concentration of Mdv1.

In addition to their biological significance, Fis1/Mdv1 and Fis1/Caf4 complexes also display distinctive structural features. TPR motif is widely involved in protein–protein interactions. The interface between known TPR-containing proteins and their partner proteins/peptides are located only in the concave surface formed by TPR motifs (18). In contrast, both TPR surfaces of Fis1 are used to bind ligands. This binding mode increases the interaction interface between the two proteins, resulting in stabilization of the complex. The Fis1/Mdv1 and Fis1/Caf4 structures therefore reveal the versatility of the TPR fold in mediating protein–protein interactions.

A central issue concerning mitochondrial fission is whether mammalian Fis1 functions in the same manner as yeast Fis1 to recruit Drp1 (the mammalian ortholog of Dnm1) to mitochondria. During apoptosis, Drp1 recruitment is enhanced, resulting in activation of mitochondrial fission during the early stages of cell death (9, 10). Sequence alignment indicates that many of the yeast Fis1 residues contacted by the adaptors are conserved in mammalian Fis1 [supporting information (SI) Fig. 5*A*]. Whereas these Fis1 orthologs have an overall identity of 24%, residues involved in ligand binding are 44% identical. In addition, a comparison of yeast and human Fis1 structures suggests that both binding grooves are conserved (SI Fig. 5 *B* and *C*). This suggests that mammalian Fis1 has a protein ligand that binds in a similar manner as Mdv1/Caf4 to yeast Fis1. Our results therefore identify residues on the surface of mammalian Fis1 likely to mediate ligand binding and will facilitate efforts to

CELL BIOLOGY

identify the mechanism of Drp1 recruitment to mitochondria during apoptosis. Moreover, they will likely facilitate efforts to manipulate mitochondrial fission artificially.

Methods

Cloning and Protein Expression. Fis1 (1–129) was amplified by PCR (primers, 5′-AAAAACATATGACCAAAGTAGATTTT-TGG-3′ and 5′-TTTTTCTCGAGGAGTGTTTCCTTCTG-GAT-3′), digested with NdeI and EcoRI, and cloned into the corresponding sites in the pBB75 vector. Mdv1 (122–171) was amplified by PCR (primers, 5′-GCACATATGGATGCAGAT-GGCAAGCTTCTA-3′ and 5′-GCCGGATCCCTAATAGTT-TAATCTTTCAGTGTTTTC-3′), digested with NdeI and BamHI, and cloned into the NdeI/BglII sites of the pET15 vector, which encodes an N-terminal His_6 tag. In a similar strategy, Caf4 (81–140) was amplified (primers, 5′-GGGAT-CATATGCAGAAAGGACAAGTAGGG-3′ and 5′-GCCA-GATCTCTATCTCTGTTGAATGATGGAAACGG-3′) and cloned into the pET15 vector.

Fis1/Mdv1 and Fis/Caf4 complexes coexpressed in Rosetta (DE3) cells were purified by Ni^{2+}–nitrilotriacetic acid chromatography, followed by cleavage of the His tag with thrombin. The protein complexes were further purified to >95% purity with ion exchange and gel filtration chromatography. The purified protein complexes were dialyzed into 20 mM Tris (pH 8).

Crystallization and Structure Determination. All of the crystallization trials were carried out at 22°C by using the hanging-drop vapor diffusion method. One microliter of the protein complex was mixed with an equal volume of reservoir solution and equilibrated against 400-μl reservoir solution. The reservoir solution for the Fis1/Mdv1 crystals contained 20% PEG3350 and 0.1 mM Tris (pH 8.0). The reservoir solution for the Fis1/Caf4 crystals contained 16% PEG3350 and 0.2 mM NaH_2PO_4. Phases were determined by molecular replacement by using the NMR structure of yeast Fis1 (24) as the starting model. Details of the crystallographic analysis and statistics are presented in Table 1.

Yeast Two-Hybrid Assay. Fis1 (1–127) was cloned into the EcoRI and BglII sites of pGAD-C1. Mdv1 (1–300), Mdv1 (88–108), Mdv1 (142–164), Mdv1 (88–164), Caf4 (1–251), Caf4 (90–109), Caf4 (122–142), and Caf4 (90–142) were cloned into EcoRI and BglII sites of pGBDU-C1. Mdv1 (301–714) and Caf4 (251–659) were cloned into the ClaI and SalI sites of pGBDU-C1. Two-hybrid analysis was performed as described previously (15). pGAD-C1 vectors containing cytosolic portion of Fis1 were transformed into PJ69–4α cells. pGBDU-C1 vectors containing Mdv1 and Caf4 fragments were transformed into PJ69–4a cells. Transformants for each vector were mated on YPD plates. Diploids were selected by replica plating to SD plates lacking leucine, uracil, and lysine. Positive interactions were detected by growing on replica SD plates lacking adenine, leucine, uracil, and lysine.

Coimmunoprecipitation. Wild-type and mutants of Myc-Fis1, HA-Mdv1, and HA-Caf4 were expressed from endogenous promoters in integrating vectors. The transformed yeast cells were grown in yeast extract/peptone/dextrose media and harvested at an OD_{600} of ≈1.0. Coimmunoprecipitations were performed as described previously (15). Briefly, the cells were lysed by using glass beads. The cleared cell lysate was applied to 9E10-conjugated protein A–Sepharose beads and incubated at 4°C for 90 min. The cell lysates and eluted protein were subjected to Western blotting by using 9E10 hybridoma supernatant (anti-Myc) or 12CA5 ascites fluid (anti-HA).

Mitochondrial Morphology Analysis. Yeast strains for morphology analysis contained mitochondrially targeted GFP or DsRed. Cells were grown to midlog phase and fixed by 3.7% formaldehyde at 30°C for 10 min. The cells were washed four times with PBS and scored for mitochondrial morphology. To determine the localization of Mdv1 mutants, mutations were introduced into the plasmid pRS416MET25 + GFP–MDV1 (a gift from J. M. Shaw, University of Utah, Salt Lake City, UT) and analyzed in yeast expressing mito-DsRed. In Fis1 mutant cells, GFP–Dnm1 localization was scored by comparison with mito-DsRed. When >50% of GFP–Dnm1 puncta were on mitochondria, it was scored as mitochondrially localized.

We thank Dr. J. M. Shaw for providing the GFP–Mdv1 vector, Priscilla Tee for technical assistance, and Erik Griffin (The Johns Hopkins University, Baltimore, MD) and Takumi Koshiba (Kyushu University, Fukuoka, Japan) for some expression constructs. Diffraction data were collected at the Stanford Synchrotron Radiation Laboratory. This work was supported by National Institutes of Health Grants GM062967 and GM083121 (to D.C.C.). Y.Z. was supported by an Elizabeth Ross postdoctoral fellowship.

1. Chan DC (2006) *Annu Rev Cell Dev Biol* 22:79–99.
2. Okamoto K, Shaw JM (2005) *Annu Rev Genet* 39:503–536.
3. Waterham HR, Koster J, van Roermund CW, Mooyer PA, Wanders RJ, Leonard JV (2007) *N Engl J Med* 356:1736–1741.
4. Verstreken P, Ly CV, Venken KJ, Koh TW, Zhou Y, Bellen HJ (2005) *Neuron* 47:365–378.
5. Fannjiang Y, Cheng WC, Lee SJ, Qi B, Pevsner J, McCaffery JM, Hill RB, Basanez G, Hardwick JM (2004) *Genes Dev* 18:2785–2797.
6. Jagasia R, Grote P, Westermann B, Conradt B (2005) *Nature* 433:754–760.
7. Abdelwahid E, Yokokura T, Krieser RJ, Balasundaram S, Fowle WH, White K (2007) *Dev Cell* 12:793–806.
8. Goyal G, Fell B, Sarin A, Youle RJ, Sriram V (2007) *Dev Cell* 12:807–816.
9. Frank S, Gaume B, Bergmann-Leitner ES, Leitner WW, Robert EG, Catez F, Smith CL, Youle RJ (2001) *Dev Cell* 1:515–525.
10. Youle RJ, Karbowski M (2005) *Nat Rev Mol Cell Biol* 6:657–663.
11. Fekkes P, Shepard KA, Yaffe MP (2000) *J Cell Biol* 151:333–340.
12. Mozdy AD, McCaffery JM, Shaw JM (2000) *J Cell Biol* 151:367–380.
13. Tieu Q, Nunnari J (2000) *J Cell Biol* 151:353–366.
14. Cerveny KL, Jensen RE (2003) *Mol Biol Cell* 14:4126–4139.
15. Griffin EE, Graumann J, Chan DC (2005) *J Cell Biol* 170:237–248.
16. Karren MA, Coonrod EM, Anderson TK, Shaw JM (2005) *J Cell Biol* 171:291–301.
17. Tieu Q, Okreglak V, Naylor K, Nunnari J (2002) *J Cell Biol* 158:445–452.
18. D'Andrea LD, Regan L (2003) *Trends Biochem Sci* 28:655–662.
19. Abe Y, Shodai T, Muto T, Mihara K, Torii H, Nishikawa S, Endo T, Kohda D (2000) *Cell* 100:551–560.
20. Gatto GJ, Jr, Geisbrecht BV, Gould SJ, Berg JM (2000) *Nat Struct Biol* 7:1091–1095.
21. Scheufler C, Brinker A, Bourenkov G, Pegoraro S, Moroder L, Bartunik H, Hartl FU, Moarefi I (2000) *Cell* 101:199–210.
22. Dohm JA, Lee SJ, Hardwick JM, Hill RB, Gittis AG (2004) *Proteins* 54:153–156.
23. Suzuki M, Jeong SY, Karbowski M, Youle RJ, Tjandra N (2003) *J Mol Biol* 334:445–458.
24. Suzuki M, Neutzner A, Tjandra N, Youle RJ (2005) *J Biol Chem* 280:21444–21452.
25. Naylor K, Ingerman E, Okreglak V, Marino M, Hinshaw JE, Nunnari J (2006) *J Biol Chem* 281:2177–2183.